Electronic Supplementary Material (ESI) for Analytical Methods.

Supporting Information

Nanoplasmonic Sensor Array for Detection and Discrimination of Pesticide Residues in Citrus

M. Reza Mirghafouri[a], Samira Abbasi-Moayed[a], Forough Ghasemi[b,*], M. Reza Hormozi-Nezhad[a,*]

[a]Department of Chemistry, Sharif University of Technology, Tehran, 11155-9516, Iran

[b]Department of Nanotechnology, Agricultural Biotechnology Research Institute of Iran (ABRII), Agricultural Research, Education, and Extension Organization (AREEO), Karaj, 3135933151, Iran

*Corresponding authors:

Forough Ghasemi, email: forough.ghasemi@abrii.ac.ir
ORCID iD: 0000-0003-1093-2058

M. Reza Hormozi-Nezhad, email: hormozi@sharif.edu
ORCID iD: 0000-0002-7472-1850

Table of contents

Content	Page
Fig. S1. Chemical structure of (a) bifenazate (BF), (b) azinphos-methyl (AM), (c) paraquat (PQ), (d) thiometon (TM), and (e) parathion-methyl (PM) pesticides.	**4S**
Fig. S2. UV–Vis spectrum, intensity size distribution, and TEM image of citrate-capped (CT) AuNPs (a, b, c, respectively), and borohydride-capped (BH) AuNPs (d, e, f, respectively)	**5S**
Fig. S3. The stability of (a) CT-AuNPs (0.5 nmol L^{-1} in the presence of citrate buffer pH 4.5), and (b) BH-AuNPs (0.224 µmol L^{-1} in the presence of phosphate buffer pH 8.0) over time	**6S**
Fig. S4. Time-course variation in UV-Vis spectra of the sensing element (a) CT AuNPs, and (b) BH AuNPs upon the addition of TM at a concentration of 100 ng mL^{-1}. The effect of incubation time (as bar plot) on the aggregation of the sensing element (c) CT-AuNPs, and (d) BH-AuNPs. The signal (A_{700}/A_{520}) is defined as the ratio of absorbance values at wavelength 700 and 520 nm, respectively.	**7S**
Fig. S5. Absorbance spectra of the sensing element (a) CT-AuNPs and (b) BH-AuNPs before and after exposure to different concentrations of bifenazate (BF) ranging from 20-5000 ng mL^{-1}	**8S**
Fig. S6. Absorbance spectra of the sensing element (a) CT-AuNPs and (b) BH-AuNPs before and after exposure to different concentrations of paraquat (PQ) ranging from 20-5000 ng mL^{-1}	**9S**
Fig. S7. Absorbance spectra of the sensing element (a) CT-AuNPs and (b) BH-AuNPs before and after exposure to different concentrations of azinphos-methyl (AM) ranging from 20-5000 ng mL^{-1}	**10S**
Fig. S8. Absorbance spectra of the sensing element (a) CT-AuNPs and (b) BH-AuNPs before and after exposure to different concentrations of thiometon (TM) ranging from 20-5000 ng mL^{-1}	**11S**
Fig. S9. Absorbance spectra of the sensing element (a) CT-AuNPs and (b) BH-AuNPs before and after exposure to different concentrations of parathion-methyl (PM) ranging from 20-5000 ng mL^{-1}	**12S**
Fig. S10. Intensity size distribution of the sensing element CT-AuNPs (a) before, and after exposure to 200 ng mL^{-1} of (b) BF, (c) PQ, (d) AM, (e) TM, and (f) PM	**13S**
Fig. S11. Intensity size distribution of the sensing element BH-AuNPs (a) before, and after exposure to 200 ng mL^{-1} of (b) BF, (c) PQ, (d) AM, (e) TM, and (f)	**14S**
Fig. S12. Absorbance response patterns (bar plots) of the sensing elements (CT- and BH-AuNPs) against BF, PQ, AM, TM, and PM pesticides at different concentrations ranging from 20-5000 ng mL^{-1} at six wavelengths of 768, 702, 634, 591, 562, and 466 nm	**15S**

Fig. S13. Heat map of the sensing elements (CT- and BH-AuNPs) against BF, PQ, AM, TM, and PM pesticides at different concentrations ranging from 20-5000 ng mL^{-1} at six wavelengths of 768, 702, 634, 591, 562, and 466 nm **16S**

Table S1. Leave-one-out analysis by Jackknifing in the linear discriminant analysis (LDA); each group contains eight concentrations of the pesticides (BF, PQ, AM, TM, and PM) with three replicates. **17S**

Fig. S14. Predicted vs. nominal plots from PLS- regression method for (a) BF, (b) PQ, (c) AM, (d) TM, and (e) PM pesticides **18S**

Fig. S15. Absorbance spectra of the sensing element (a) CT-AuNPs and (b) BH-AuNPs before and after exposure to a total concentration of 100 ng mL^{-1} of PQ, AM, and their mixtures **19S**

Fig. S16. (a) Two-dimensional score plot discriminating the mixtures of PQ and AM with different percentage (total concentration was 100 ng mL^{-1}), and (b) canonical variable 1 (from part a) plotted versus the percentage of PQ **20S**

Table S2. Leave-one-out analysis by Jackknifing in the linear discriminant analysis (LDA); each group contains a mixture of PQ and AM in different percentage with three replicates. **21S**

Fig. S17. Absorbance response patterns (bar plots) of the sensing elements (CT- and BH-AuNPs) against the mixtures of PQ and AM with different percentage (total concentration was 100 ng mL^{-1}) at six wavelengths of 768, 702, 634, 591, 562, and 466 nm **22S**

Fig. S18. Heat map of the sensing elements (CT- and BH-AuNPs) against the mixtures of PQ and AM with different percentage (total concentration was 100 ng mL^{-1}) at six wavelengths of 768, 702, 634, 591, 562, and 466 nm **23S**

Table S3. Identification of unknown pesticides in the lime samples based on the calculation of Mahalanobis distance of each unknown from the centroid of training groups. LDA was performed on the data matrix containing the test set data (BF, PQ, AM, TM, and PM at concentrations 200 ng mL^{-1} with three replicates in the real sample of lime) and the training set data (BF, PQ, AM, TM, and PM at concentrations 60, 80, 100, 200, 400, 600, 800, and 1000 ng mL^{-1} with three replicates). **24S**

Table S4. A list of NP-based sensor arrays for the identification of pesticides (OP= organophosphate, CB= carbamate, BP= bipyridylium) **25S**

References **26S**

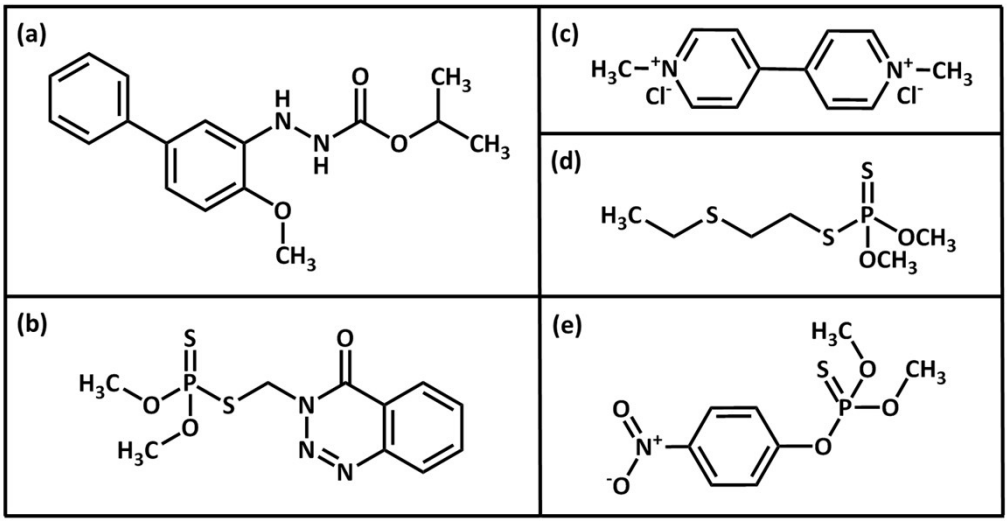

Fig. S1. Chemical structure of (a) bifenazate (BF), (b) azinphos-methyl (AM), (c) paraquat (PQ), (d) thiometon (TM), and (e) parathion-methyl (PM) pesticides.

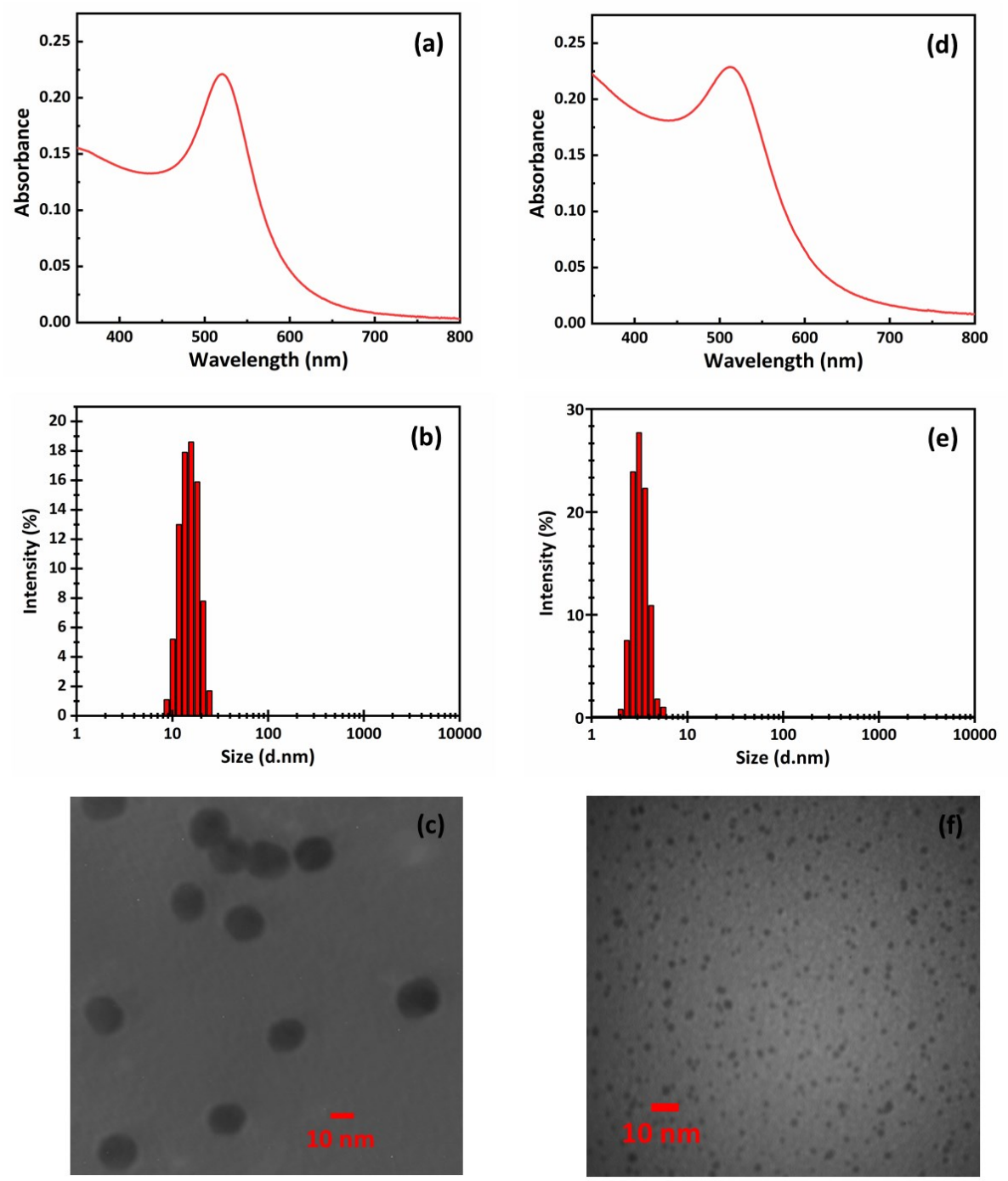

Fig. S2. UV–Vis spectrum, intensity size distribution, and TEM image of citrate-capped (CT) AuNPs (a, b, c, respectively), and borohydride-capped (BH) AuNPs (d, e, f, respectively)

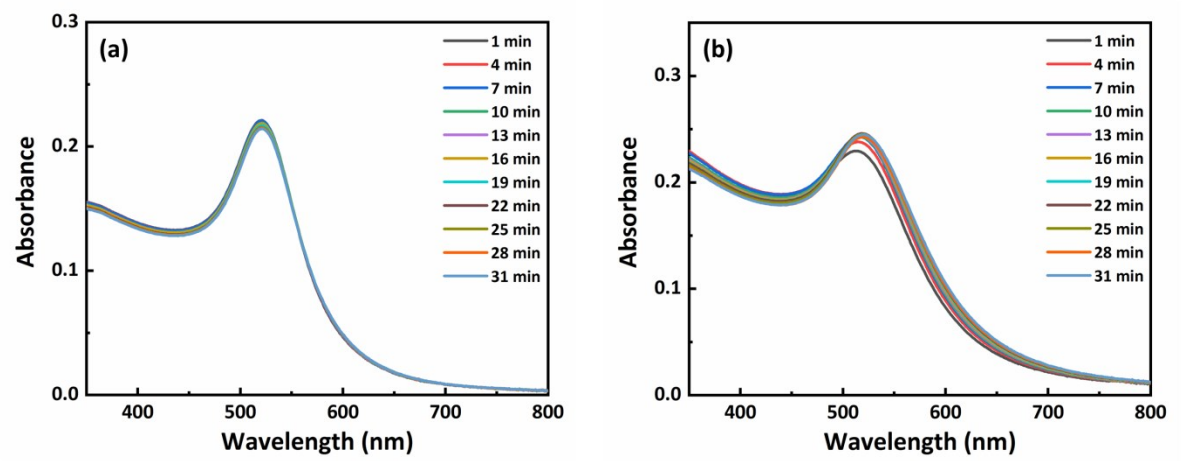

Fig. S3. The stability of (a) CT-AuNPs (0.5 nmol L^{-1} in the presence of citrate buffer pH 4.5), and (b) BH-AuNPs (0.224 µmol L^{-1} in the presence of phosphate buffer pH 8.0) over time

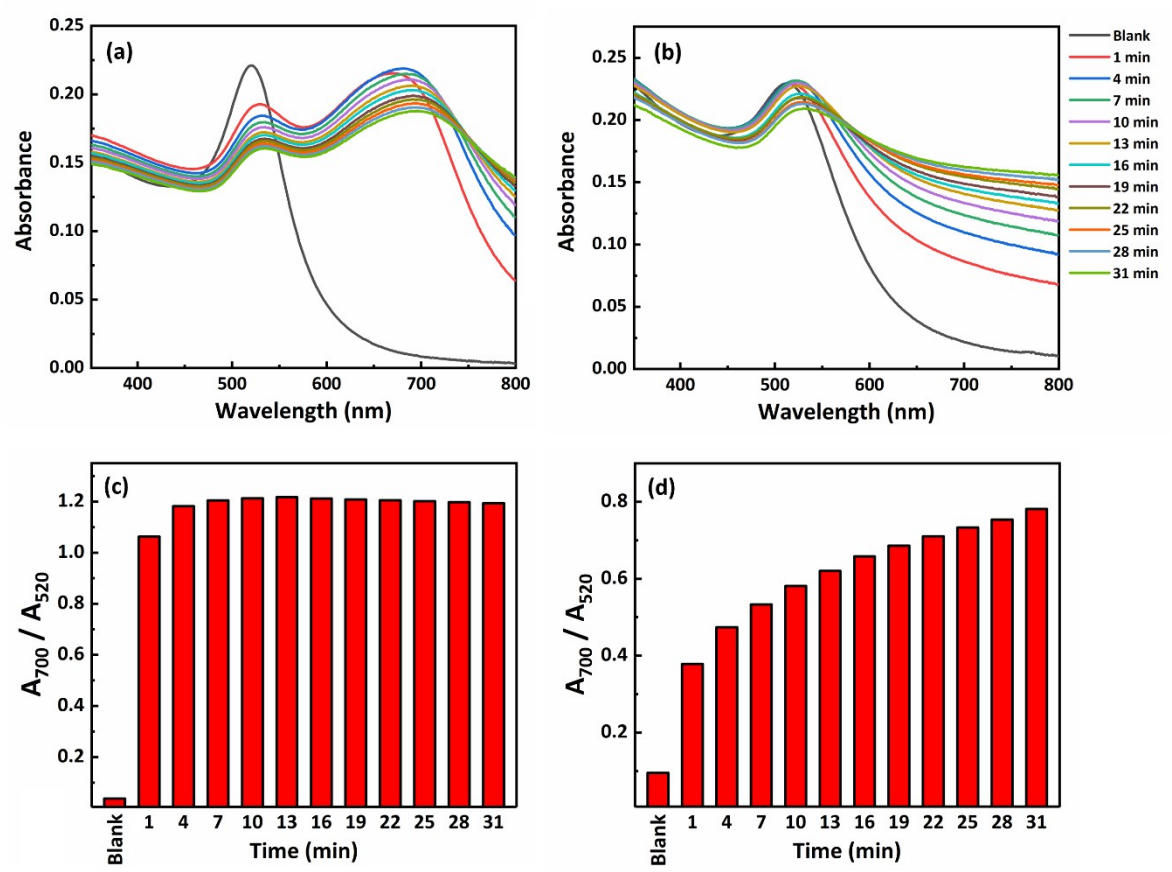

Fig. S4. Time-course variation in UV-Vis spectra of the sensing element (a) CT AuNPs, and (b) BH AuNPs upon the addition of TM at a concentration of 100 ng mL^{-1}. The effect of incubation time (as bar plot) on the aggregation of the sensing element (c) CT-AuNPs, and (d) BH-AuNPs. The signal (A_{700}/A_{520}) is defined as the ratio of absorbance values at wavelength 700 and 520 nm, respectively.

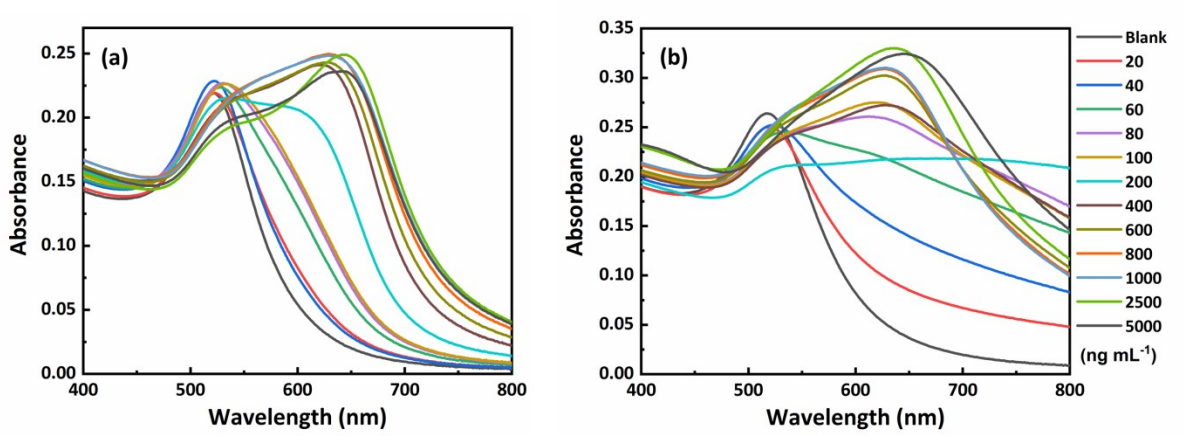

Fig. S5. Absorbance spectra of the sensing element (a) CT-AuNPs and (b) BH-AuNPs before and after exposure to different concentrations of bifenazate (BF) ranging from 20-5000 ng mL^{-1}

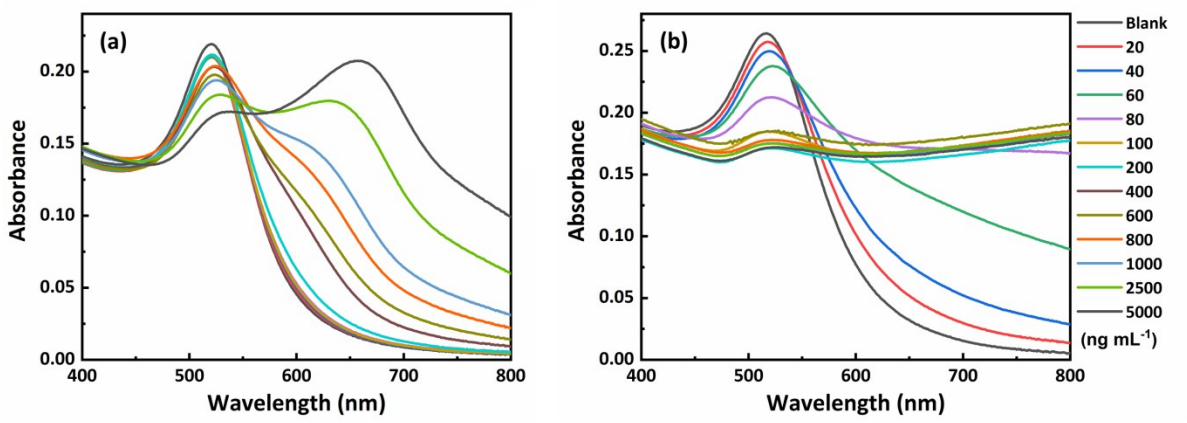

Fig. S6. Absorbance spectra of the sensing element (a) CT-AuNPs and (b) BH-AuNPs before and after exposure to different concentrations of paraquat (PQ) ranging from 20-5000 ng mL^{-1}

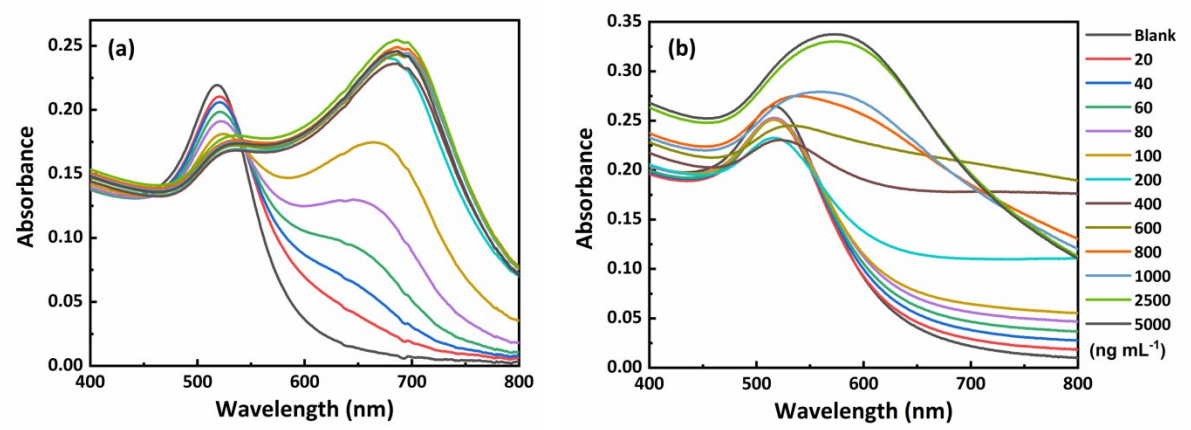

Fig. S7. Absorbance spectra of the sensing element (a) CT-AuNPs and (b) BH-AuNPs before and after exposure to different concentrations of azinphos-methyl (AM) ranging from 20-5000 ng mL^{-1}

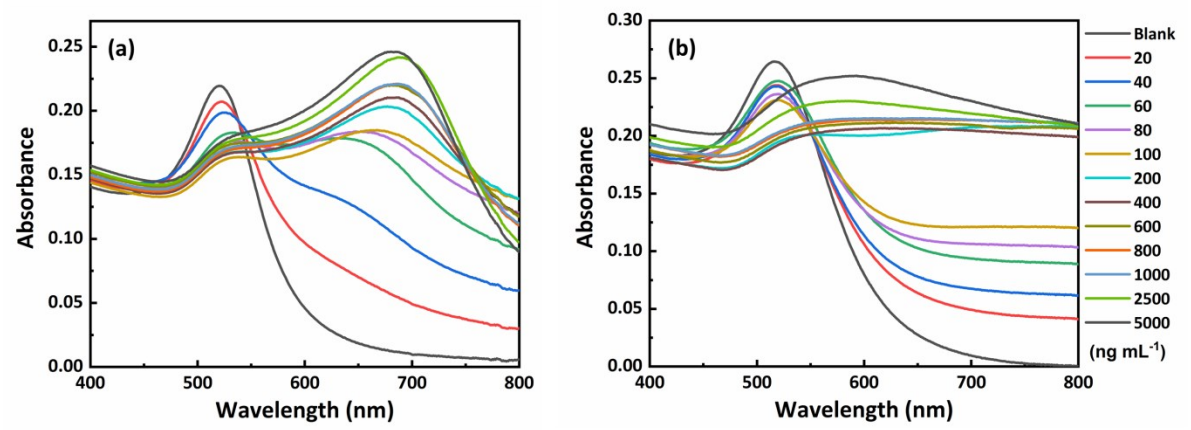

Fig. S8. Absorbance spectra of the sensing element (a) CT-AuNPs and (b) BH-AuNPs before and after exposure to different concentrations of thiometon (TM) ranging from 20-5000 ng mL^{-1}

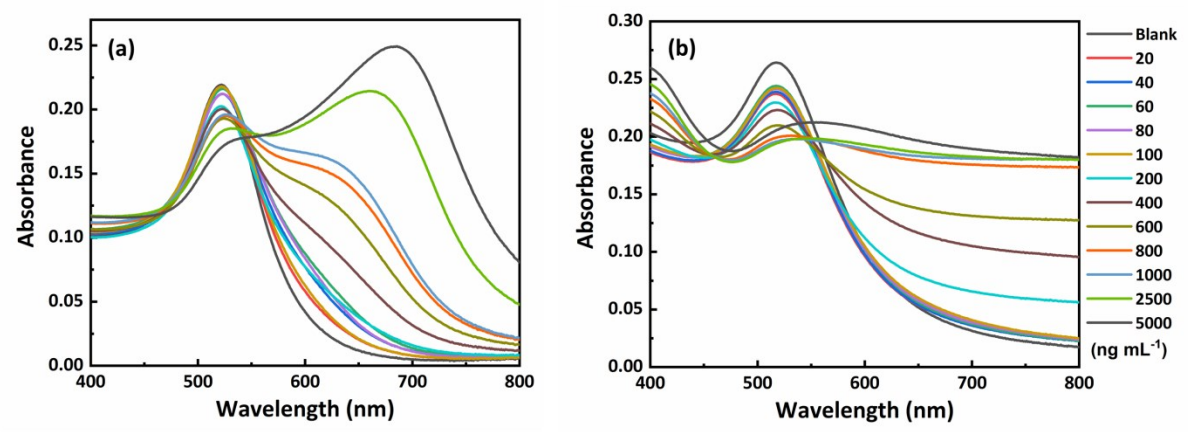

Fig. S9. Absorbance spectra of the sensing element (a) CT-AuNPs and (b) BH-AuNPs before and after exposure to different concentrations of parathion-methyl (PM) ranging from 20-5000 ng mL^{-1}

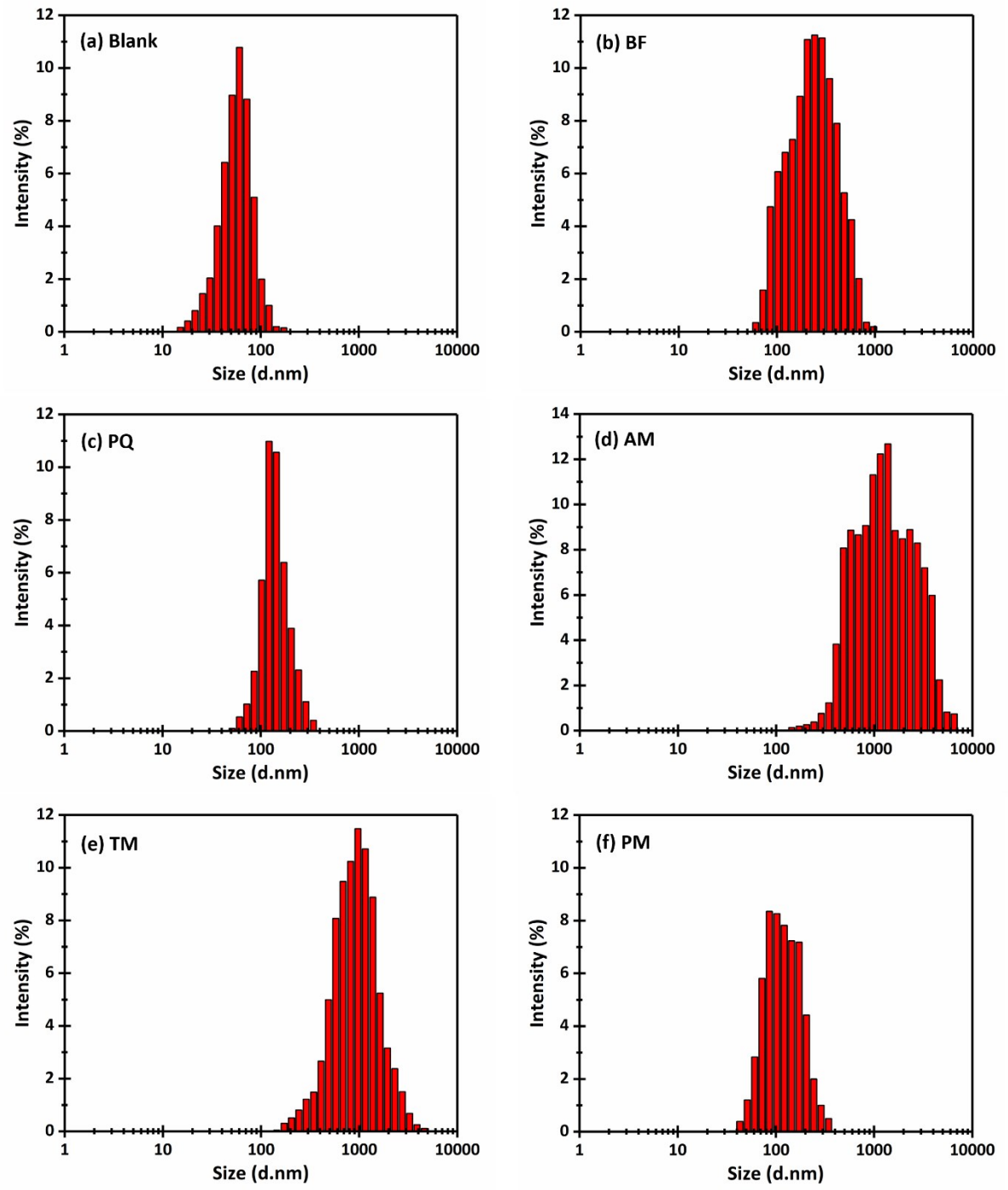

Fig. S10. Intensity size distribution of the sensing element CT-AuNPs (a) before, and after exposure to 200 ng mL^{-1} of (b) BF, (c) PQ, (d) AM, (e) TM, and (f) PM

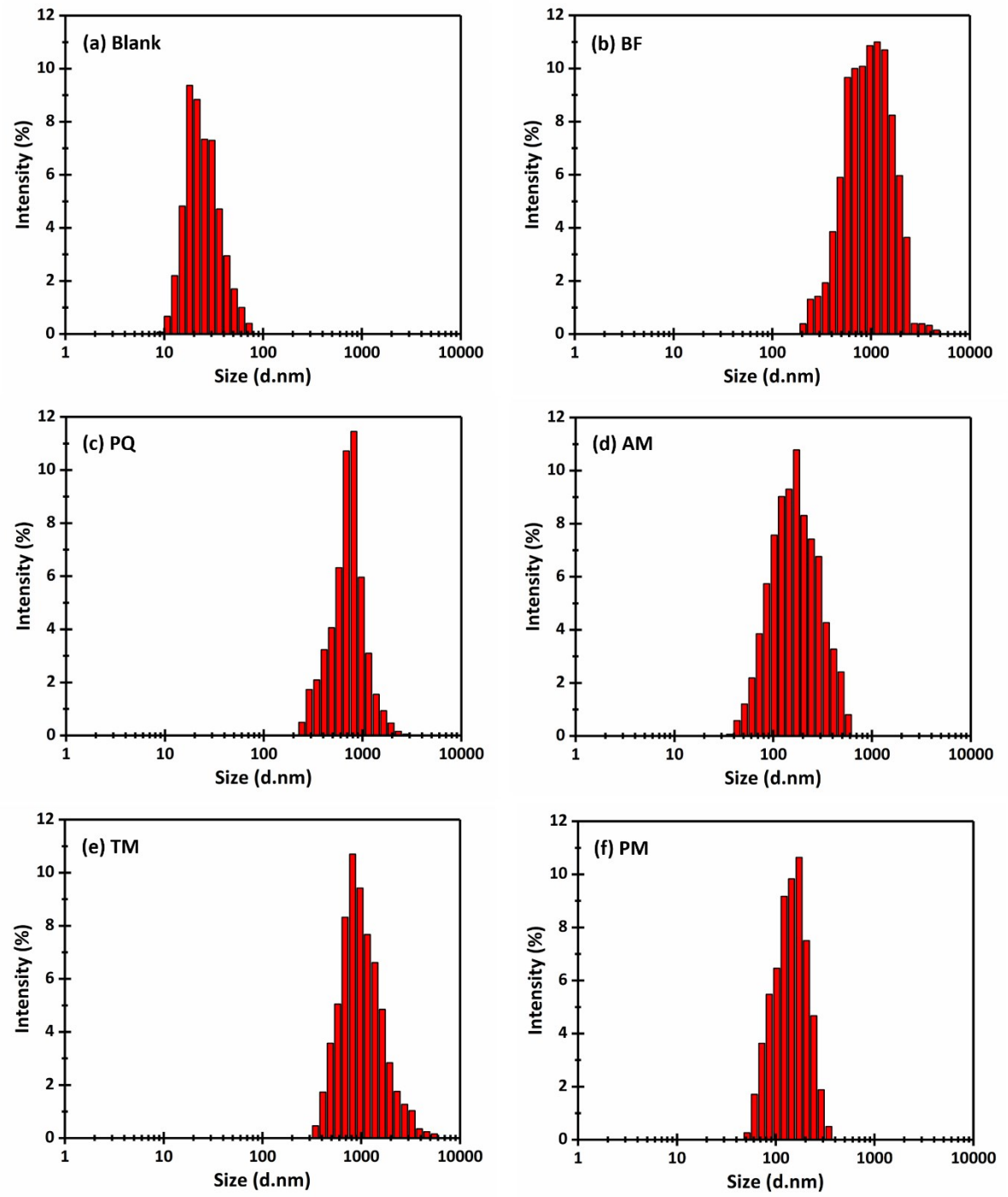

Fig. S11. Intensity size distribution of the sensing element BH-AuNPs (a) before, and after exposure to 200 ng mL^{-1} of (b) BF, (c) PQ, (d) AM, (e) TM, and (f) PM

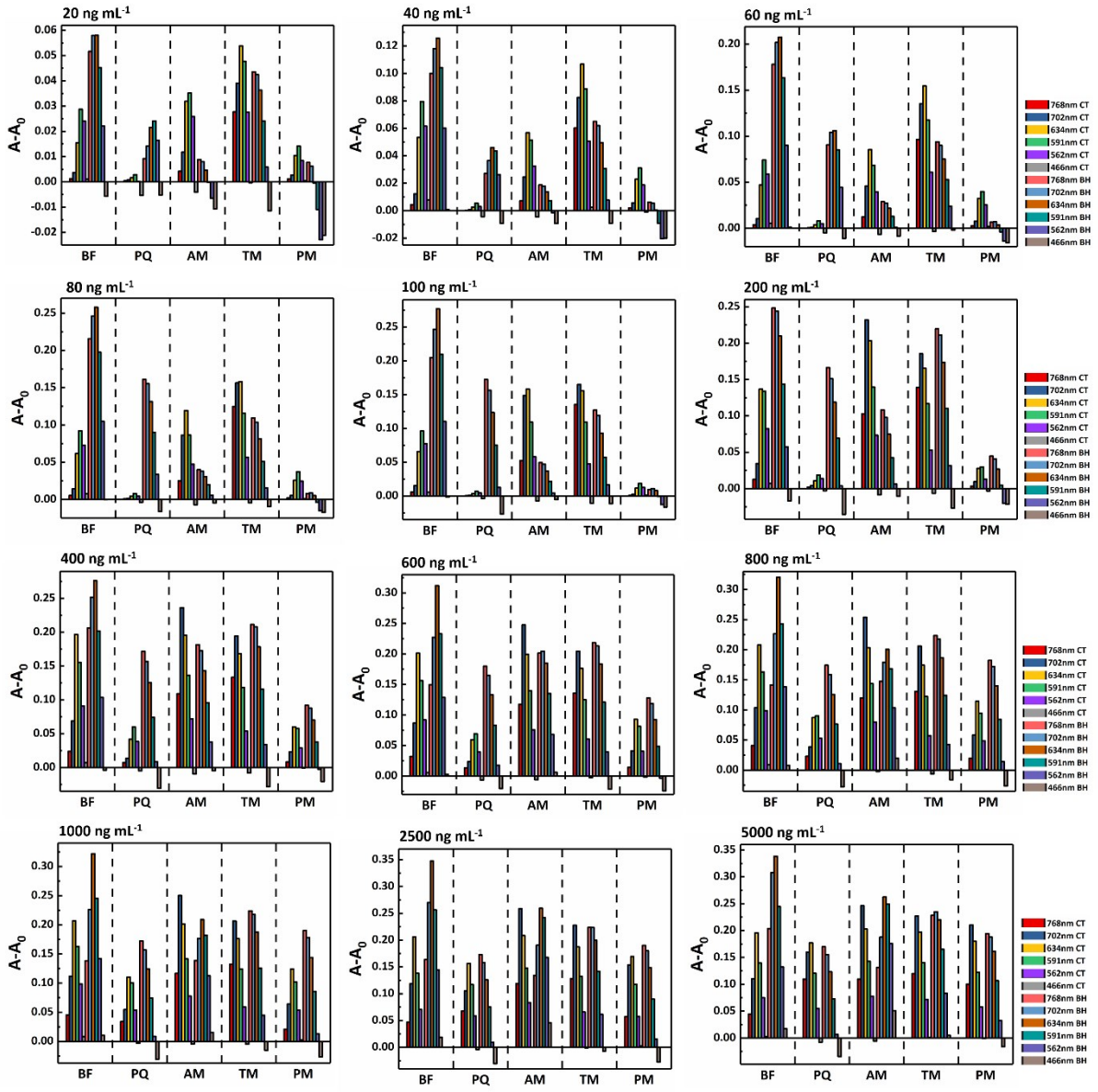

Fig. S12. Absorbance response patterns (bar plots) of the sensing elements (CT- and BH-AuNPs) against BF, PQ, AM, TM, and PM pesticides at different concentrations ranging from 20-5000 ng mL^{-1} at six wavelengths of 768, 702, 634, 591, 562, and 466 nm

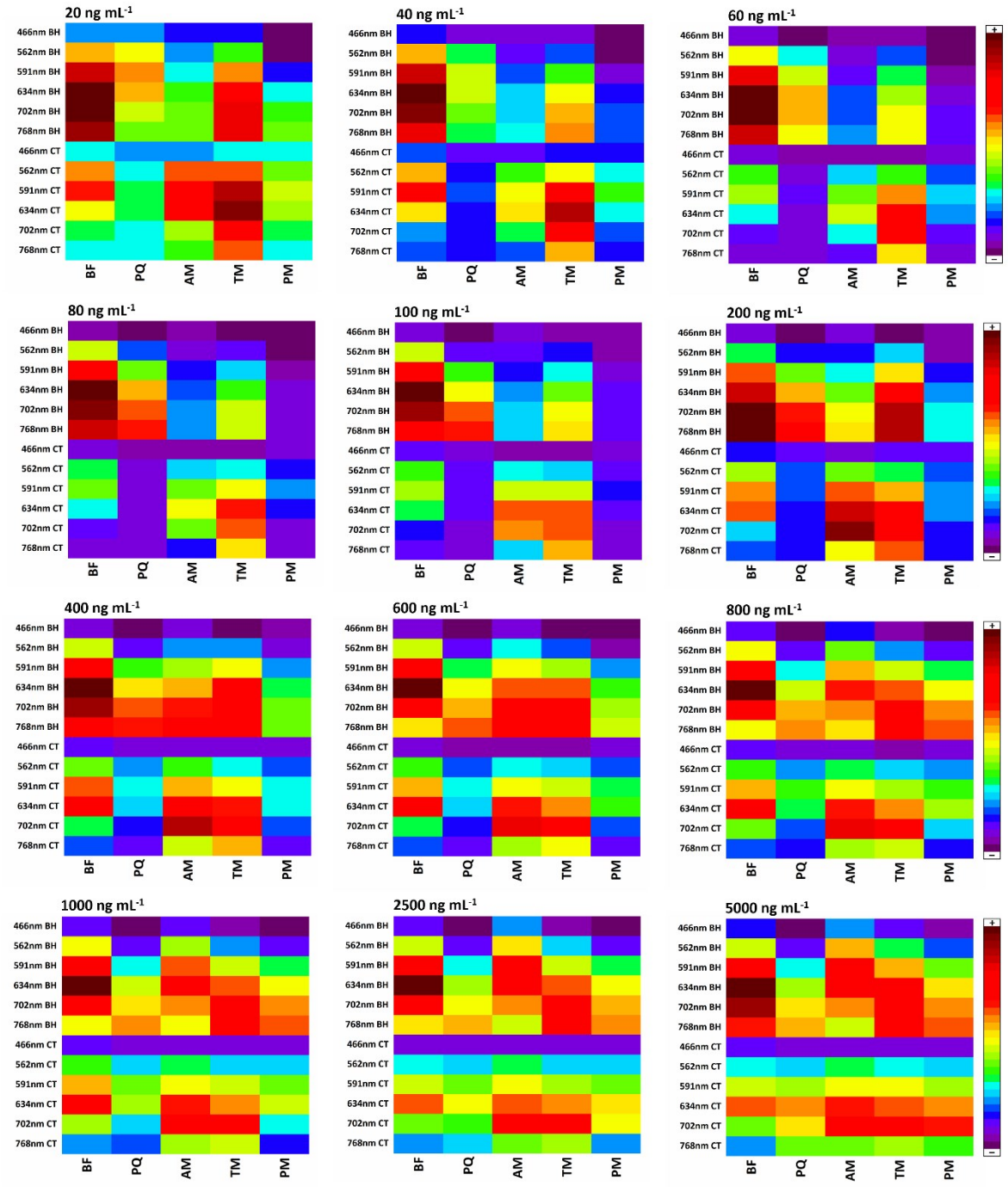

Fig. S13. Heat map of the sensing elements (CT- and BH-AuNPs) against BF, PQ, AM, TM, and PM pesticides at different concentrations ranging from 20-5000 ng mL^{-1} at six wavelengths of 768, 702, 634, 591, 562, and 466 nm

Table S1. Leave-one-out analysis by Jackknifing in linear discriminant analysis (LDA); each group contains eight concentrations of the pesticides (BF, PQ, AM, TM, and PM) with three replicates.

	Predicted Group					
	BF	PQ	AM	TM	PM	Total
BF	24	0	0	0	0	24
	100.00%	0.00%	0.00%	0.00%	0.00%	100.00%
PQ	0	24	0	0	0	24
	0.00%	100.00%	0.00%	0.00%	0.00%	100.00%
AM	0	0	24	0	0	24
	0.00%	0.00%	100.00%	0.00%	0.00%	100.00%
TM	0	0	0	24	0	24
	0.00%	0.00%	0.00%	100.00%	0.00%	100.00%
PM	0	0	0	0	24	24
	0.00%	0.00%	0.00%	0.00%	100.00%	100.00%
Total	24	24	24	24	24	120
	20.00%	20.00%	20.00%	20.00%	20.00%	100.00%

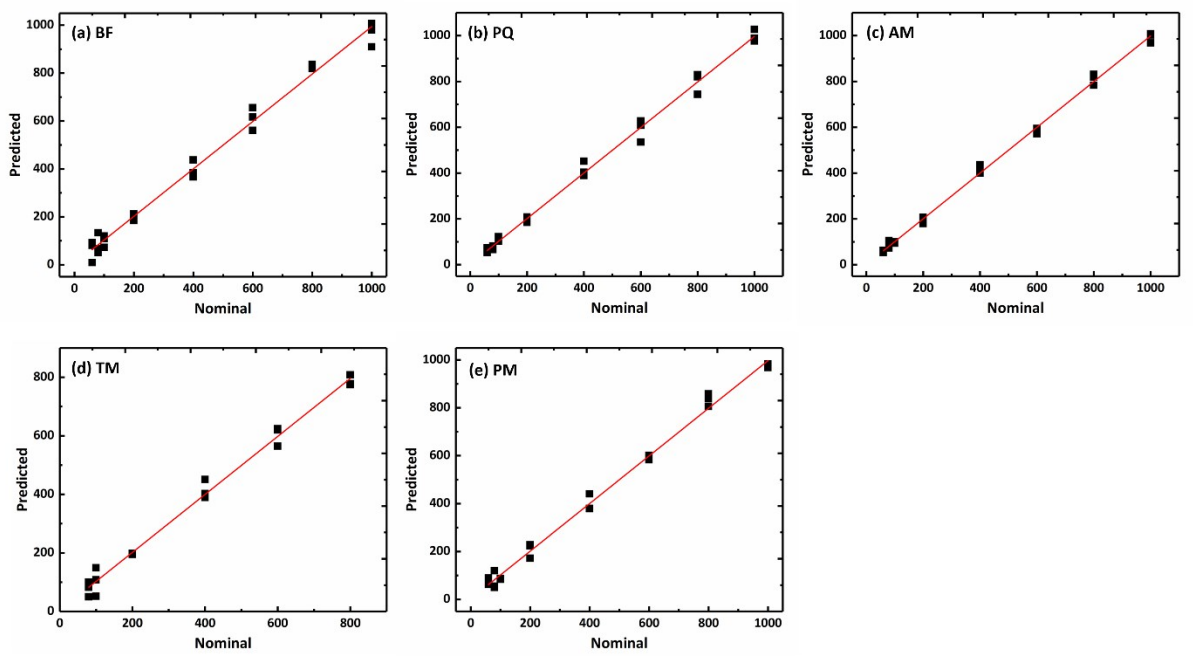

Fig. S14. Predicted vs nominal plots from PLS- regression method for (a) BF, (b) PQ, (c) AM, (d) TM, and (e) PM pesticides

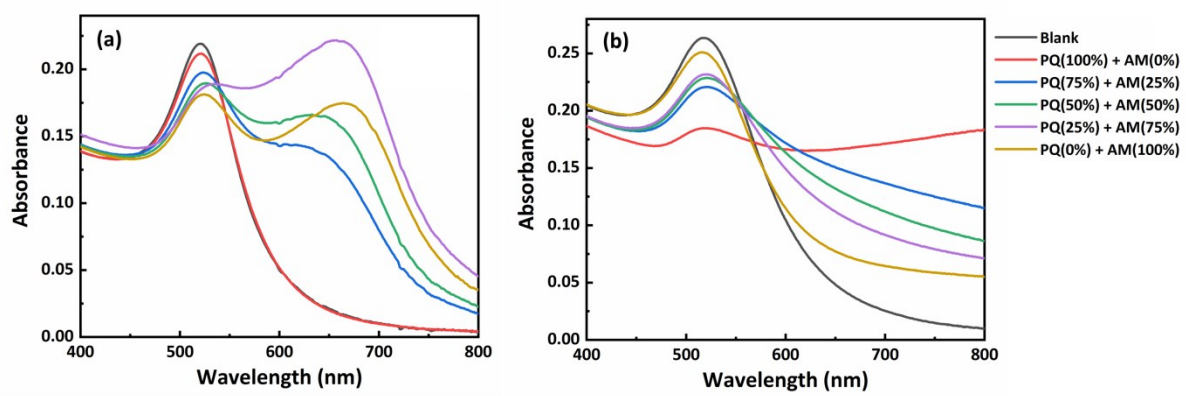

Fig. S15. Absorbance spectra of the sensing element (a) CT-AuNPs and (b) BH-AuNPs before and after exposure to a total concentration of 100 ng mL^{-1} of PQ, AM, and their mixtures

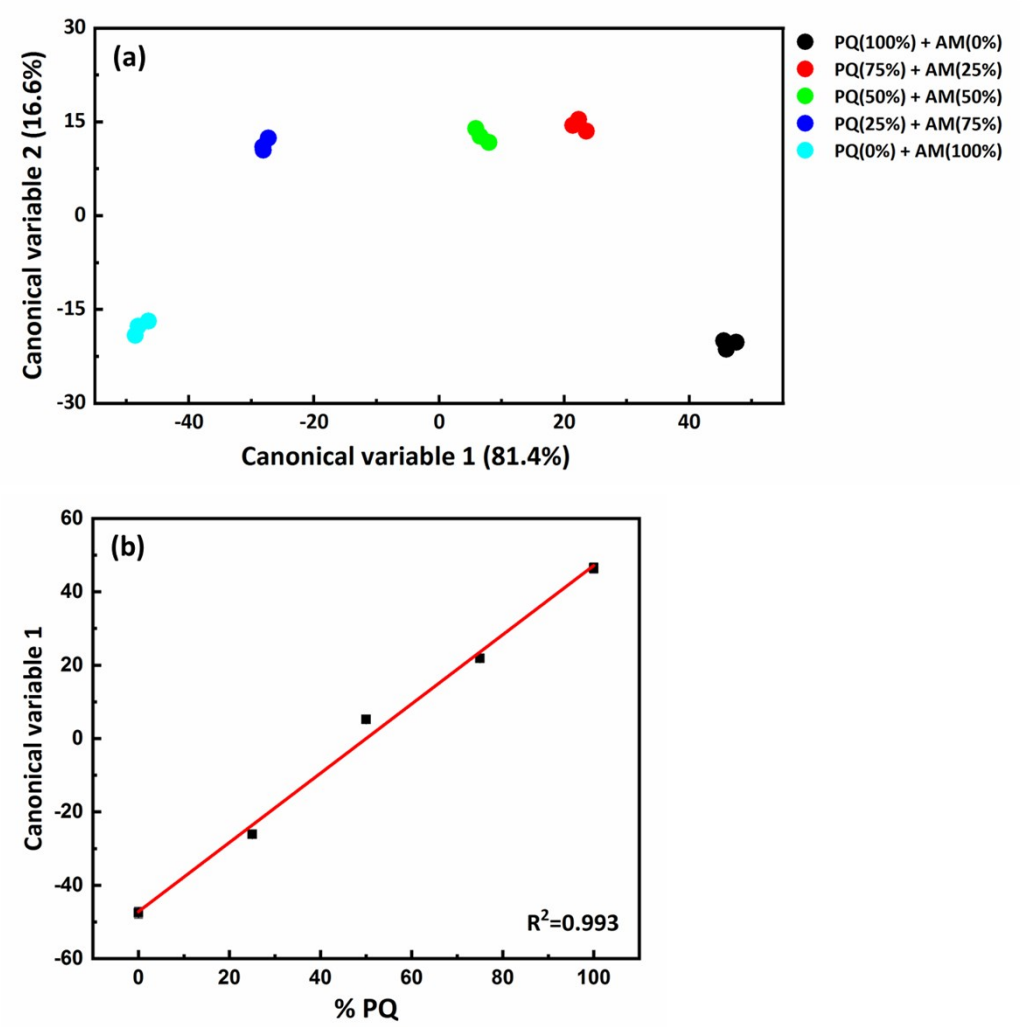

Fig. S16. (a) Two-dimensional score plot discriminating the mixtures of PQ and AM with different percentage (total concentration was 100 ng mL^{-1}), and (b) canonical variable 1 (from part a) plotted versus the percentage of PQ

Table S2. Leave-one-out analysis by Jackknifing in the linear discriminant analysis (LDA); each group contains a mixture of PQ and AM in different percentage with three replicates.

	Predicted Group					
	PQ(100%) + AM(0%)	PQ(75%) + AM(25%)	PQ(50%) + AM(50%)	PQ(25%) + AM(25%)	PQ(0%) + AM(100%)	Total
PQ(100%) + AM(0%)	3	0	0	0	0	3
	100.00%	0.00%	0.00%	0.00%	0.00%	100.00%
PQ(75%) + AM(25%)	0	3	0	0	0	3
	0.00%	100.00%	0.00%	0.00%	0.00%	100.00%
PQ(50%) + AM(50%)	0	0	3	0	0	3
	0.00%	0.00%	100.00%	0.00%	0.00%	100.00%
PQ(25%) + AM(25%)	0	0	0	3	0	3
	0.00%	0.00%	0.00%	100.00%	0.00%	100.00%
PQ(0%) + AM(100%)	0	0	0	0	3	3
	0.00%	0.00%	0.00%	0.00%	100.00%	100.00%
Total	3	3	3	3	3	15
	20.00%	20.00%	20.00%	20.00%	20.00%	100.00%

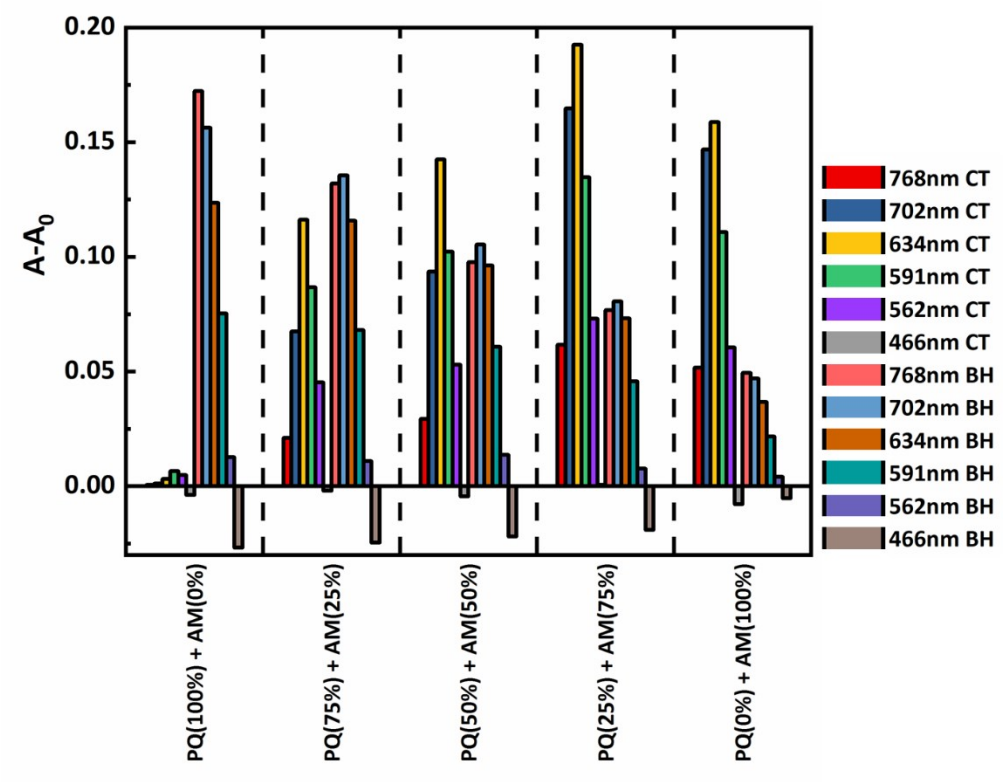

Fig. S17. Absorbance response patterns (bar plots) of the sensing elements (CT- and BH-AuNPs) against the mixtures of PQ and AM with different percentage (total concentration was 100 ng mL^{-1}) at six wavelengths of 768, 702, 634, 591, 562, and 466 nm

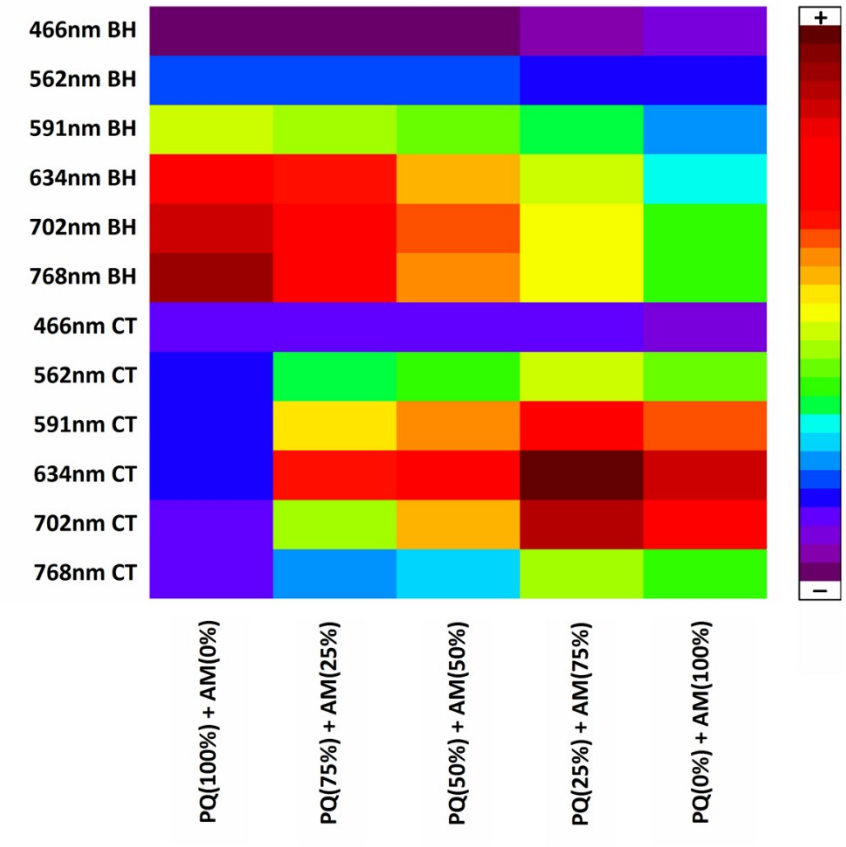

Fig. S18. Heat map of the sensing elements (CT- and BH-AuNPs) against the mixtures of PQ and AM with different percentage (total concentration was 100 ng mL^{-1}) at six wavelengths of 768, 702, 634, 591, 562, and 466 nm

Table S3. Identification of unknown pesticides in the lime samples based on the calculation of Mahalanobis distance of each unknown from the centroid of training groups. LDA was performed on the data matrix containing the test set data (BF, PQ, AM, TM, and PM at concentrations 200 ng mL^{-1} with three replicates in the real sample of lime) and the training set data (BF, PQ, AM, TM, and PM at concentrations 60, 80, 100, 200, 400, 600, 800, and 1000 ng mL^{-1} with three replicates).

Sample	Mahalanobis distance-square					Identified	Accuracy of identification
	BF	PQ	AM	TM	PM		
1	45.36131	126.78796	191.99359	220.96947	148.91471	BF	Yes
2	43.87954	102.55999	179.75357	201.1711	122.80454	BF	Yes
3	41.31105	105.64168	171.08573	195.18349	128.08483	BF	Yes
4	201.51787	72.82814	104.69993	82.05639	108.03062	PQ	Yes
5	148.62868	30.36855	104.35081	84.85261	53.23868	PQ	Yes
6	158.33014	42.2233	101.75719	72.24844	70.39314	PQ	Yes
7	226.2669	103.72279	57.81268	122.6263	95.87441	AM	Yes
8	231.91045	116.8669	69.16256	139.09023	126.0507	AM	Yes
9	224.01716	107.03395	57.07736	134.00643	98.64147	AM	Yes
10	289.85886	142.2333	267.26395	52.80494	160.24572	TM	Yes
11	263.1207	113.72233	184.61032	28.78659	157.80008	TM	Yes
12	276.24597	118.68355	200.77878	26.0917	163.33792	TM	Yes
13	138.59799	39.6375	100.57843	99.1637	26.56069	PM	Yes
14	150.72512	48.9046	130.41298	122.77771	30.78778	PM	Yes
15	166.55147	58.26904	142.73798	138.36148	48.16191	PM	Yes

Table S4. A list of NP-based sensor arrays for the identification of pesticides (OP= organophosphate, CB= carbamate, BP= bipyridylium)

Target pesticides	Group	Discriminated concentrations (ng mL^{-1})	Sensing elements	Ref.
Azinphos-methyl	OP	120-400	AuNPs at different pHs and different NaCl concentrations (nine sensing elements)	[1]
Chlorpyrifos	OP			
Fenamiphos	OP			
Pirimiphos-methyl	OP			
Phosalone	OP			
Azinphos-methyl	OP	50-800	AgNPs at different pHs (three sensing elements)	[2]
Phosalone	OP			
Bifenazate	CB	20-5000	AuNPs with different surface coating (two sensing elements)	This work
Paraquat	BP			
Azinphos-methyl	OP			
Thiometon	OP			
Parathion-methyl	OP			

References

1. N. Fahimi-Kashani and M. R. Hormozi-Nezhad, *Anal. Chem.*, 2016, **88**, 8099-8106.

2. A. Orouji, S. Abbasi-Moayed and M. R. Hormozi-Nezhad, *Spectrochim. Acta A*, 2019, **219**, 496-503.